Published in final edited form as:

Cancer Res. 2019 April 01; 79(7): 1465–1479. doi:10.1158/0008-5472.CAN-18-1972.

STING promotes homeostasis via regulation of cell proliferation and chromosomal stability

Diana Rose E. Ranoa[1], **Ryan C. Widau**[1], **Stephen Mallon**[1], **Akash D. Parekh**[1], **Claudia M. Nicolae**[2], **Xiaona Huang**[1], **Michael J. Bolt**[1], **Ainhoa Arina**[1], **Renate Parry**[3], **Stephen J. Kron**[4,5], **George-Lucian Moldovan**[2], **Nikolai N. Khodarev**[1,5,*], and **Ralph R. Weichselbaum**[1,5,*]

[1]Department of Radiation and Cellular Oncology, The University of Chicago, Chicago, IL 60637

[2]Department of Biochemistry and Molecular Biology, The Pennsylvania State University College of Medicine, 500 University Drive, Hershey, PA 17033

[3]Translational Medicine, Varian Medical Systems Inc., Palo Alto, CA

[4]Department of Molecular Genetics and Cellular Biology, The University of Chicago, Chicago, IL 60637

[5]The Ludwig Center for Metastasis Research, The University of Chicago, Chicago, IL 60637

Abstract

Given the integral role of Stimulator of interferon genes (STING, *TMEM173*) in the innate immune response, its loss or impairment in cancer is thought to primarily affect antitumor immunity. Here we demonstrate a role for STING in the maintenance of cellular homeostasis through regulation of the cell cycle. Depletion of STING in human and murine cancer cells and tumors resulted in increased proliferation compared to wild-type controls. Microarray analysis revealed genes involved in cell cycle regulation are differentially expressed in STINGko compared to WT MEFs. STING-mediated regulation of the cell cycle converged on NF-κB- and p53-driven activation of p21. The absence of STING led to premature activation of cyclin-dependent kinase 1 (CDK1), early onset to S phase and mitosis, and increased chromosome instability, which was enhanced by ionizing radiation (IR). These results suggest a pivotal role for STING in maintaining cellular homeostasis and response to genotoxic stress.

Keywords

cell cycle regulation; CDKN1A; chromosomal instability (CIN); ionizing radiation; Stimulator of interferon genes (STING/TMEM173)

[*]Corresponding authors Ralph R. Weichselbaum, The University of Chicago Medicine, 5758 S. Maryland Ave., MC 9006, Chicago, IL 60637, Phone: 773-702-0817, Fax: 773-834-7233, rrw@radonc.uchicago.edu, Nikolai N. Khodarev, The University of Chicago, Knapp Center for Biomedical Discovery, 900 East 57th St., Room 6144, Chicago, IL 60637, Phone: 773-834-3282, Fax: 773-702-1968, n-khodarev@uchicago.edu.

Conflict of Interest: R.C. Widau is a clinical research scientist and has ownership interest (including stock, patents, etc.) in Eli Lilly and Company. R. Parry has ownership interest (including stock, patents, etc.) in Varian Medical Systems. S.J. Kron reports receiving commercial research grant from AbbVie and has ownership interest (including stock, patents, etc.) in OncoSenescence. R.R. Weichselbaum has ownership interest (including stock, patents, etc.) in OncoSenescence and Boost Therapeutics Inc. No potential conflicts of interest were disclosed by the other authors.

Introduction

Stimulator of IFN genes (STING, also known as TMEM173, MITA, ERIS, and MPYS) is a cytoplasmic pattern recognition receptor shown to be an important transducer of Type I interferon (IFN) production triggered by the accumulation of double stranded DNA (dsDNA) in the cytoplasm. STING is localized in the endoplasmic reticulum (ER) and following activation dimerizes, undergoes conformational changes, and translocates to the ER-Golgi intermediate compartments(1–3). STING induces phosphorylation of TANK-binding kinase 1 (TBK1), leading to a signaling cascade involving IRF3 and NF-κB and the production of type I IFNs(1,2,4,5). STING directly mediates innate immune responses to cyclic dinucleotides produced by intracellular bacteria and viruses(2,6) as well as the endogenous cyclic dinucleotide cGAMP (c[G(2’−5’)pA(3’−5’)p])(7,8). cGAMP is a second messenger synthesized by the enzyme cGAS, which serves as the primary cytoplasmic dsDNA sensor in metazoans(8–10).

Ionizing radiation (IR) is associated with double-stranded DNA (dsDNA) breaks, affecting cellular proliferation and survival(11). The acute DNA damage and changes in growth factors and/or chemokine levels activate intracellular stress sensors that signal cell cycle progression or inhibition depending on the balance of damage and growth factors(12). Defects in subsequent DNA repair can result in accumulation of chromosomal aberrations(13). Recently, it has been demonstrated that genotoxic stress-induced DNA damage leads to the formation of micronuclei and/or chromosomal fragments that are recognized by cGAS following loss of nuclear compartmentalization, triggering cellular senescence through STING-mediated production of type I IFN and other pro-inflammatory cytokines(14–18).

STING serves a key role in initiation of immune responses against tumors(19). Several studies have shown that recruitment of tumor-infiltrating host immune cells via STING activation mediates IR-triggered anti-tumor immune responses(19–21). It has been recently demonstrated that innate immune sensing by dendritic cells following radiotherapy is dominated by the cGAS and STING-dependent cytosolic DNA sensing pathway, which drives the adaptive immune response to ionizing radiation(21).

Interestingly, cancer cells often display inactivated STING(22,23). For example, screening seventeen different histological types of tumors from ~8,000 patients, Uhlén *et al.*(24) observed significant heterogeneity of STING expression. It remains unclear what selective advantage cancer cells might gain by downregulating STING pathway function. Here we demonstrate that STING also serves homeostatic roles in cell growth and proliferation analogous to those of a tumor suppressor, serving as a brake on cell division and maintaining genomic stability. STING constrains cell proliferation and entry to mitosis via NF-κB- and p53-driven activation of the stoichiometric cyclin-dependent kinase inhibitor CDKN1A (p21, WAF1, CIP1). Loss of STING promotes premature entry to S phase and mitosis, resulting in smaller cell size and increased chromosomal instability (CIN). Radiation potentiates the chromosomal instability. Our findings suggest a function for STING during

normal cell division in protecting cells against aneuploidy, serving as a barrier to tumorigenesis.

Materials and Methods

Animals

All animal studies had been approved by the Institutional Animal Care and Use Committee (IACUC) of the University of Chicago (Protocol number 72213). Mice were maintained under specific pathogen-free conditions in a barrier facility. Age-matched 6–8 weeks old female C57BL/6 or athymic nude mice were purchased from Harlan. STINGko mice were acquired from Dr. Glen N. Barber (University of Miami).

Cell lines

Wild-type and STINGko primary mouse embryonic fibroblasts (MEFs) were derived from 13.5 days post-coitus embryos and cultured in DMEM supplemented with 10% FBS and 1% non-essential amino acids for no more than five passages(25). MEFs were immortalized with a retrovirus expressing SV40-large T antigen (Addgene plasmid 13970). $p50^{-/-}$ primary MEFs were kindly provided by Dr. Giovanna Bernal (University of Chicago). Normal human dermal adult fibroblast primary cell line (HDFA), Human embryonic kidney 293 (HEK293, accession ID: CVCL_0045), human colon adenocarcinoma HCT116 (ID: CVCL_0291), and lung adenocarcinoma A549 (ID: CVCL_0023) were purchased from ATCC. Human glioblastoma D54 (ID: CVCL_7185) was obtained from Dr. Daryll D. Bigner (Duke University Medical Center), while the murine colon adenocarcinoma MC-38 (ID: CVCL_B288) derived from C57BL/6 mice was obtained from Dr. Xuanming Yang (University of Chicago). SCC61 (ID: CVCL_7118) was isolated from human head and neck squamous cell carcinoma (PMID 3458227). Cell lines were submitted to IDEXX BioAnalytics (Columbia, MO) for authentication using STR profiling. The cells were cultivated as follows: SCC61 in DMEM/F12 with 20% FBS and 1% HC (hydrocortisone); HEK293, HCT116, and MC-38 cell lines in DMEM high glucose with 10% FBS; D54 cell line in MEM with 10% FBS, A549 cell line in DMEM/F12 with 10% FBS, and HDFA in Fibroblast growth kit with low serum (2%), 5ng/ml EGF, 50ug/ml L-glutamine, 1ug/ml hydrocortisone, and 5ug/ml insulin. All cell lines used were routinely screened for mycoplasma contamination using the Lonza MycoAlert Mycoplasma Detection Kit (CN LT07–418). Only cells from early passage frozen stocks were used for the experiments.

In vivo tumor model and IR exposure for cell lines in vitro

Human tumor xenografts (1×10^6 cells) were established in the right flank of athymic nude mice, while 1×10^6 MC-38 tumor cells were subcutaneously injected at the back of C57BL/6 mice. For each experiment, up to 5 animals are housed per cage and assigned an ear tag number. Each animal (i.e. technical replicates) in the cage were administered the same treatment. Tumor volumes were measured along 3 orthogonal axes and calculated using the formula for an ellipsoid [(l x w x h)/2]. Tumor growth was measured, recorded, and monitored by a single investigator every 3–4 days for the entire duration of the experiment in order to ensure consistency of measurement. Tumor growth was quantitatively calculated by extrapolating the linear equation of the growth curve from each measurement to compute for

the time for each tumor to reach an arbitrarily assigned volume (300 cubic mm). Mice were sacrificed when tumor sizes reached a volume of 2000–3000 mm^3. Cell lines maintained in tissue culture were irradiated using a Gammacell 220 (MDS Nordion, Ottawa, Canada) ^{137}Cs γ-irradiator.

Cell doubling time calculation

Cells were seeded at 10,000 cells/well in 24-well plates. At several time points (24, 48, 72, 96, and 120 hours) post-seeding, cells were counted using a TC20 automated cell counter (Bio-Rad). Data was plotted as the logarithm of the number of viable cells over time. The growth rate was calculated by extrapolating the slope of the line from the exponential portion of the semilog growth curves. Alternatively, we calculated the doubling time of cells by fitting the linear data to the equation of exponential growth: N(t) = N(0) e^(kt) with k as the growth rate constant and N(t) and N(0) the number of cells at time t and time 0, respectively, using the *Exponential Growth* analysis function in GraphPad Prism software. Doubling time was calculated from the formula ln(2)/k.

Live cell imaging and analysis

Cells were seeded in 24-well plates at a density of 25,000 cells per well in appropriate growth media and incubated overnight to allow monolayer formation. Thirty minutes prior to IR treatment, media was replaced with fresh growth media containing the nuclear stain Incucyte NucLight Rapid Red Reagent (Essen BioScience, Ann Arbor, MI) for live cell imaging at 1:3000 dilution. Following irradiation, the plates were placed into either the IncuCyte ZOOM or IncuCyte S3 apparatus and images of the collective cell spreading are recorded every 4 hours for a total duration of 48–72 hours. For each cell line tested and treatment conditions, we performed three identically prepared experimental replicates (n=3), and experiments were repeated 3–4 times. Basic analyses were performed using the IncuCyte software to plot phase confluence, calculate the number of nuclei-stained cells, and measure the average nuclei area over time. In some experiments, the WEE1 kinase inhibitor MK1775 (Axon Medchem, Reston, VA) was added to fresh media at a final concentration of 250 nmol/L together with the NucLight Rapid Red Reagent prior to IR treatment.

Stable shRNA-mediated STING knockdown

Tumor cell lines were transfected with shSTING construct within a TRC2-pLKO-puro vector backbone (Sigma-Aldrich mission shRNA) using Fugene HD transfection reagent at 1:3 plasmid DNA:lipid ratio. Five different shRNA constructs were tested for each human cell line (TRCN0000164628, TRCN0000160895, TRCN0000163296, TRCN161052, and TRCN0000163029), while three shRNA constructs were tested for murine cell line MC-38 (TRCN0000346321, TRCN0000346319, and TRCN0000346264). The TRC2 pLKO.5-puro non-mammalian targeting shRNA (TRCN SHC002 for human cell lines and TRCN SHC202 for murine cells; Sigma-Aldrich) was used as a control. Stable lines from the top two shSTING constructs were selected by growth in culture media containing 5 μg/ml puromycin over multiple passages. Successful knockdown of STING was confirmed by Western blot (Supplementary Fig. S1A-C). Stable cell lines from mixed pools following puromycin selection were further assessed for IFN-β production, caspase 3/7 activity, and clonogenic survival as described in (25). For murine tumor models and cell growth studies,

we selected the stable cell line from the shSTING contruct that yielded the best knock-down for each cell line. The specific product numbers used for each cell line are summarized below:

D54 shSTING: TRCN0000161052

HCT116 shSTING: TRCN0000163029

SCC61 shSTING: V3LHS324286

A549 shSTING: TRCN0000163029

MC-38 shSTING: TRCN0000346319

Measurement of Cell Cycle Population by EdU/BrdU and PI double staining

To measure the percent population of actively dividing cells as well as the total DNA content of cells, a dual staining protocol using a fluorescently-conjugated anti-EdU/BrdU antibody to measure EdU/BrdU incorporation together with Propidium Iodide (PI) were performed on tumor cells with or without STING knockdown at different time points following IR treatment. Cells were seeded overnight in 6-well plates at a density of 100,000 cells/well. Cells were either mock-irradiated or exposed to 6Gy IR, and were harvested at different time points post-treatment. For pulse/chase experiments, the Click-iT Plus EdU Alexa Fluor 647 Flow Cytometry Assay Kit (Invitrogen) was used together with PI. EdU was added to cells in culture one hour prior to harvest time (for pulse experiments) or at a fixed time point (for chase experiments) at a final concentration of 0.03 μM. Cells were harvested at different time points post-labeling and processed for immunostaining following manufacturer's protocol. In the final step, cells were resuspended in PBS containing 25 μg/ml PI (eBioscience) and 100 μg/ml RNase A (Thermo Fisher). After overnight incubation at 4° C, Flow cytometry was performed to measure the number of EdU^+ cells in the Alexa Fluor 647 channel, while the number of PI-positive cells were detected in the PE channel. Analyses were gated on single cells using the FlowJo software.

For regular cell cycle experiments, the BrdU/PI staining protocol was performed. Four hours prior to harvest time, the growth media was replaced with BrdU (Invitrogen)-containing fresh media diluted at 1:100. Cells were trypsinized and carefully permeabilized with 70% ethanol for at least 30 minutes on ice. After washing with PBS, cells were incubated in 2M HCl solution for 30 minutes at room temperature. Cells were washed in PBS, followed by 2 washes using the blocking buffer (PBS + 1%BSA + 1% Tween-20). Cells were resuspended in blocking buffer and incubated with FITC-conjugated anti-BrdU monoclonal antibody (eBioscience) overnight at 4° C. The following day, cells were washed 2X with blocking buffer and resuspended in PBS containing 25 μg/ml PI (eBioscience) and 100 μg/ml RNase A (Thermo Fisher). After 1-hour incubation at 4° C, Flow cytometry was performed to measure the number of FITC-conjugated anti-BrdU antibody that bound to actively dividing cells (S phase) in one channel, while the number of PI-positive cells will be used to quantify the percent population of cells in G1 and G2/M phase of the cell cycle in another channel. Analysis were gated on single cells using the FlowJo software.

Microarray analysis

WT and STINGko primary MEFs were seeded in 6-well plates at a density of 2×10^5 cells/well. Approximately 15 hours post-seeding, cells were either mock-irradiated (un-irradiated) or exposed to 6 Gy IR. Total RNA was isolated using Trizol reagent following the manufacturer's protocol. RNA yield was measured using Qubit RNA broad range kit. 100 ng of RNA was labeled per the manufacturer's instructions and profiled in duplicate using the Illumina Mice WG-6 array (Illumina, San Diego CA). Background subtraction and quantile normalization was performed across arrays using Illumina Beadstudio software. Analysis was performed as described in (25).

siRNA-mediated knockdown of CDKN1A in HCT116 and MEFs cells

HCT116 and MEFs cell lines were transiently transfected with specific siRNA constructs to CDKN1A (Dharmacon). Non-targeting siRNA was used as a control (Dharmacon D-001210-02-05). Twenty-four hours post-transfection, cells were either mock-irradiated or exposed to increasing doses of IR. Cells were then assayed for Western blot and cell cycle analysis using dual BrdU/PI staining and flow cytometry. The two siRNA constructs that successfully knocked down CDKN1A in HCT116 and MEFs cells, respectively, are:

siRNA to human CDKN1A: GAUGGAACUUCGACUUUGU (Dharmacon D-003471-01)

siRNA to murine CDKN1A: CGAGAACGGUGGAACUUUG (Dharmacon D-058636-01)

In some experiments with wild-type MEFs, STING was transiently knocked-down, either alone or in combination with p21, using the siGENOME mouse TMEM173 siRNA with sequence CGAAAUAACUGCCGCCUCA (Dharmacon M-024333-00).

Fluorescence microscopy and CBMN Assay

Wild-type and STINGko MEFs were plated overnight in 2-well chambered slides (at 20,000 cells/chamber). Cells were either mock-irradiated or exposed to either 6Gy or 12Gy IR. At different time points post-IR treatment (24 or 48 hours), MitoTracker Red (Invitrogen) was added to cells and incubated at 37ºC for 1 hour. Cells were washed with PBS and fixed in 3.7% paraformaldehyde for 10 minutes and washed 2X with PBS. Cells were then permeabilized with 70% ethanol for 1 hour at 4° C followed by 2X PBS wash. Cell nuclei were stained with Draq5 solution (Abcam) diluted in PBS to a final concentration of 2 μM, and incubated at RT for 30 minutes. After final washing steps (2X PBS), cells were mounted in Prolong Gold (Thermo Fisher). Cells were visualized using Leica SP5 2-Photon Confocal microscope at 63X magnification. Fifteen images were collected per variable tested. Approximately n=150 cells were analyzed per condition.

For the cytokinesis-block micronucleus (CBMN) assay(26), Cytochalasin B (Sigma) dissolved in DMSO was added to each chamber well at a final concentration of 1.5 μg/ml, 24 hours post-IR treatment. After an additional 24 hours incubation at 37° C, MitoTracker Red (Invitrogen) was added to cells and incubated at 37° C for an additional hour. Cells

were then processed and imaged as described above. At least n=50 binucleated cells were analyzed for the CBMN assay.

Karyotyping

Primary wild-type and STINGko MEFs at Passage 1 were seeded in T-25 flasks at approximately 750,000 cells in DMEM + 10% FBS media + 1% non-essential amino acids. Fifteen hours post-seeding, cells were either mock-irradiated or exposed to 6 Gy IR. Live cells were shipped to Cell Line Genetics (Madison, WI) and were fixed for karyotype analysis at approximately 48 hours post-IR treatment.

Chromatin Immunoprecipitation (ChIP)

Stable HCT116 cell lines expressing short hairpin RNAs targeting STING (shSTING) or scrambled control (shScrambled) were transiently transfected with siRNA targeting CDKN1A or scrambled control. Twenty-four hours post-transfection, selected cells were irradiated at 9Gy and incubated for an additional 24 hours. Chromatin was then extracted from 2×10^6 cells for ChIP using the Chromatin Immunoprecipitation Assay Kit (Sigma Millipore, CN 17–295). Briefly, following chromatin crosslinking with 1% formaldehyde for 10 minutes at 37^{o}C and sonication, the anti-E2F4 antibody (Santa Cruz Biotech, sc-398543) was used for immunoprecipitation, and chromatin washes were performed as per the kit. Chromatin was eluted in 100ul of elution buffer (1% SDS, 100mM NaHCO3). Cross-linking was reversed by incubating the samples overnight at 65^{o}C with 200mM NaCl and 200mg/ml Proteinase K. DNA was purified with Monarch PCR and DNA Cleanup Kit (New England Biolabs). Quantitative PCR using iTaq Universal SYBR Green Supermix (Bio-Rad) was the utilized to determine E2F4 binding at the BUB1, MAD2L1, and GAPDHS promoters using the following primer sequences:

BUB1 Forward primer: 5’-GAG GGA GGT GGG ACT TGA C-3’

BUB1 Reverse primer: 5’-CAA ACC TGA ACC GCA AAC TA-3’

MAD2L1 Forward primer: 5’-CCA CAG CTT TAC AGG GTT CG-3’

MAD2L1 Reverse primer: 5’-ACC TTA TTC CTG TCC TGC CC-3’

GAPDH Forward primer: 5’-AGA CCA GCC TGA GCA AAA GA-3’

GAPDH Reverse primer: 5’-CTA GGC TGG AGT GCA GTG GT-3’

HEK293 and HCT116 reconstitution experiments

HEK293 or HCT116 (WT or $p53^{-/-}$) cells were seeded in a 24-well plate overnight at a density of 75,000 cells/well. Cells were co-transfected with either an NF-κB promoter-driven luciferase reporter or a p65 binding site-mutant CDKN1A promoter-driven reporter construct(27) together with a Renilla luciferase gene driven by a basal promoter (pRL-null) as a transfection control. Transfections were performed using a cationic lipid agent, Fugene-HD (Promega), at a 3:1 lipid:DNA ratio. Twenty-four hours post-transfection, cells were either mock-irradiated or exposed to 6 Gy IR. Forty-eight hours post-IR treatment, cell lysates were collected and 20 μl were transferred to opaque 96-well plates. Following the manufacturer’s protocol for the dual luciferase assay (Promega), samples were analyzed for

IFN- β luciferase and Renilla luciferase activity using Promega Glomax reader (Madison, WI). The transfection efficiency across different wells was normalized by dividing the firefly luciferase activity by the Renilla luciferase control. After correcting for transfection efficiency, all values were normalized to those of non-irradiated cells transfected with the empty pEF-BOS vector.

Western blotting antibodies

For confirmation of targeted knockdown experiments as well as transient transfection/reconstitution experiments in both murine and human cell lines, the following primary antibodies were used: anti-STING (clone D2P2F; #13647; Cell Signaling Technology), anti-cGAS (#15102 and #31659; Cell Signaling Technology), anti-p21 (ab109199; Abcam), anti-TBK1 (sc-9910; Santa Cruz Biotechnology), anti-phospho-TBK1 Ser172 (clone D52C2; #5483S; Cell Signaling Technology), anti-IRF-3 (clone FL-425; sc-9082; Santa Cruz Biotechnology), anti-phospho IRF3 Ser396 (70R-35220; Fitzgerald Antibodies), anti-STAT1 p84/p91 (clone C-136; sc-464; Santa Cruz Biotechnology), anti- NF-κB p65 (clone D14E12; #8242; Cell Signaling Technology), anti-phospho-NF-κB p65 Ser536 (clone 93H1; #3033; Cell Signaling Technology), anti-FLAG (M2 clone; Sigma), anti-CDC2 (#77055S; Cell Signaling Technology), anti-phospho-CDC2 Tyr15 (clone 10A11; #4539; Cell Signaling Technology), anti-Rb (#9313S; Cell Signaling Technology) anti-phospho-Rb Ser807/811 (clone D20B12; #8516; Cell Signaling Technology), and anti-Actin-HRP (sc-47778; Santa Cruz Biotechnology). Secondary antibodies conjugated to HRP (Cell Signaling Technology) were used at a 1:5,000 dilution.

Quantification of Western blot bands

All protein bands in Western gels were quantified using ImageJ. The pixel units obtained for each band was normalized to the pixel units calculated from their respective b-Actin loading control. For phosphorylated proteins, we then quantified the fraction of phosphorylated proteins to the absolute total amount of protein (total protein + phosphorylated protein). For dose-dependent and stimulation assays, the variables tested were normalized to their respective wild-type unstimulated controls.

Statistical analysis

For animal studies, figures are representative of ≥ 3 biological replicates and each of these experiments contains 5–6 technical replicates. For in vitro assays, data presented are representative of ≥ 3 independent experiments and each of these experiments contains three technical replicates. Data are plotted as standard error of the mean (SEM) of these replicates, with p-values calculated using a two-tailed Student’s t-test. The two-tailed Student’s t-test is a standard statistical test for measuring the significance of the results from these assays.

Data Availability

All microarray data were submitted to Gene Expression Omnibus (GEO) with accession number GSE113123.

Results

STING regulates cell growth *in vivo* and *in vitro*

We screened multiple human cancer cell lines as well as normal cells to measure their basal level of STING expression and to examine the role of STING in tumor cells. As shown in Fig. 1A top panel, STING is expressed in normal human adult primary dermal fibroblasts (HDFA), HEK293 fibroblasts, glioblastoma cell line D54, the human colorectal carcinoma HCT116, and the murine colon carcinoma MC-38, but was not detected in human A549 lung carcinoma and murine 4T1 mammary epithelial cells. The amount of STING expression from each human and murine tumor cell lines was normalized to primary cell line controls (HDFA for human and MEFs for murine cell lines, respectively). Our data suggest that for human tumor cell lines, HCT116 and SCC61 have lower protein levels of STING compared the normal HDFA cell lines. D54, on the other hand, exhibited higher STING protein level compared to control (Fig. 1A bottom panel). For murine cell lines, large T-antigen immortalization of MEFs led to an increase in STING expression while MC-38 exhibited a slightly lower STING protein level compared to primary MEFs control (Fig. 1A bottom panel). To investigate STING function in human tumor cells, we developed stable cell lines expressing short hairpin RNAs targeting STING (shSTING) or scrambled control (shScrambled) in D54, HCT116, SCC61 and MC-38, with respectively 54.2%, 82.4%, 99.98%, and 75.63% down-regulation of protein expression compared to non-targeting control. (Fig. 1B). Flank tumors formed by the shSTING human tumor cell lines in athymic nude mice or shSTING MC-38 in syngeneic C57BL/6 mice each displayed significantly more rapid tumor growth than controls (Fig. 1C–F and Table I p-value ≤ 0.05). As expected, there was no observed significant difference between A549 shScrambled and shSTING cell lines (Fig.1G and Table I, p-value = 0.659).

To assess the role of STING in cell proliferation, we measured the growth curve of normal and tumor cells *in vitro* via manual cell counting at different time points post-seeding. Growth rate was calculated by extrapolating the slope of the line from the exponential portion of the semi-log growth curves (Table II). Cell proliferation of shSTING D54, HCT116, and SCC61 human tumor cells as well as MC-38 murine tumor cells was significantly faster and have higher calculated slope, μ, than shScrambled controls (Fig. 1H–K, and Table II, p-value ≤ 0.05). Similarly, primary and immortalized mouse embryonic fibroblasts (MEFs) isolated from STINGko mice exhibited accelerated growth compared to WT control (Fig. 1L–M), suggesting the effects are not limited to transformed cells. Overall, the cell growth data indicate STING depletion confers a shorter cell doubling time compared to controls (Table II), and as expected, no difference was observed between A549 shScrambled and shSTING cell lines (Fig.1N and Table II, p-value = 0.0.577). These results confirm a previously uncharacterized role of STING in cell proliferation.

To examine the molecular mechanisms underlying deregulated growth in the absence of STING, we asked whether the absence of STING confers changes in cell cycle distribution. MEFs were treated with EdU (5-ethynyl-2'-deooxyuridine) to identify S phase cells, and fixed at the indicated time points. The EdU was labeled with azido-Alexa Fluor 647 by copper(I)-catalyzed azide-alkyne cycloaddition Click chemistry and co-stained with

propidium iodide (PI), and cells were examined by flow cytometry to distinguish G1 (2N), S and G2/M (4N) cells by DNA content. Cells were exposed to a single dose of ionizing radiation (6Gy) to induce genotoxic stress-mediated cell cycle arrest. Using the gating strategy shown in Fig.2A for data analysis, we demonstrate that, strikingly, STINGko MEFs displayed almost two-fold higher proportion of EdU+ S-phase cells versus WT controls at all time points, independent of ionizing radiation (Fig. 2B, Supplementary Fig. S2A). The greater S phase content was associated with fewer interphase cells overall, but the distributions in G1 and G2/M displayed a reciprocal pattern. STINGko MEFs displayed a decreased fraction with G2/M DNA content (Fig. 2B, $p \leq 0.05$). STINGko and WT MEFs displayed similar accumulation of cells in G2/M delay after irradiation. The fractions of unirradiated STINGko and WT MEFs in G1 were more similar across the time course, but with a slightly *increased* G1 content in STINGko MEFs (Fig. 2B). Both STINGko and WT MEFs displayed similar *depletion* of G1 content after irradiation.

To distinguish cells that were already in S phase at the time of irradiation from those entering S phase afterwards, we "chased" the EdU and measured the percent of EdU-labeled MEFs at different time points (Fig. 2C). Analyzing these cells as above and applying the gating strategy in Fig. 2D, we were able to detect a distinct population of EdU-positive cells that accumulate in the 2N G1 DNA content peak at later time points, corresponding to cells that completed mitosis during the time course (Supplementary Fig. S2B)(28). As shown in Fig. 2E, the fraction of STINGko MEFs that are at the onset of S phase (EdU^+ cells) increases at a more rapid rate than WT over time. Gating for cells newly entering S phase during the time course (Fig. 2E, S phase 2^{nd} cycle) demonstrated that in the absence of STING, cells re-enter the cell cycle earlier than WT, with or without prior irradiation.

A simple interpretation of this pattern is that STING is required to properly delay onset of cell division, allowing completion of S phase DNA replication, G2 cell growth and early events in mitosis. Deregulated mitotic entry promotes aneuploidy and polyploidy, leading to CIN(13) and mitotic catastrophe. Accordingly, loss of STING in MEFs or depletion in HCT116 tumor cells yielded a higher fraction of polyploid cells compared to their respective controls, as indicated by EdU^+ cells with greater than 4N DNA content (Figs. 2F–G). Taken together, our data suggest that STING has critical roles in maintaining proper timing of the cell cycle, with a particular defect at onset of mitosis.

STING regulates expression of the stoichiometric cyclin-dependent kinase inhibitor CDKN1A

All EdU labeling experiments shown on Figure 2 were performed at early time points post-radiation treatment (2–10 hours post-IR). Our data suggest that within this time frame, both WT and STINGko cell lines exhibited similar response to IR. However, STING has previously been reported to have a role in mediating type I IFN signaling in response to IR(4,5,21). We measured Type I IFN signaling in WT and STINGko MEFs at 48 hours post-IR exposure. As expected, STINGko MEFs fail to induce TBK1 and IRF3 phosphorylation in response to IR exposure (Fig. 3A and Supplementary Fig. S3A). Consequently, IR-induced IFN-β production is abrogated in STINGko MEFs as well as shSTING MC-38 cells

(Fig. 3B–C) while overexpression of FLAG-tagged STING in HEK293 cells led to a radiation dose-dependent increase in IFN-β promoter-driven luciferase activity (Fig. 3D).

To investigate transcriptional programs associated with STING-mediated regulation of cell cycle and response to IR, we used transcriptional profiling of STINGko and WT primary MEFs that were either mock-irradiated or exposed to 6 Gy IR. We analyzed the number of differentially expressed genes (DEGs) and found that the absence of STING led to 2,946 DEGs. Of the 367 genes differentially expressed by WT cells 48 hours after irradiation, 265 were also identified as STING-dependent genes (Fig. 3E).

As expected, functional analysis of the DEGs using Ingenuity Pathway Analysis (IPA, Qiagen) revealed that the absence of STING led to significant differential expression of genes involved in activation of IFN regulatory factors (IRF) by cytosolic pattern recognition receptors as well as IFN signaling (Fig. 3F). But prominent in the IPA analysis were canonical pathways involved in cell cycle control of chromosomal replication, chromosomal stability and segregation, and DNA damage response (Fig. 3F). To validate the cell-autonomous role of STING in DNA damage response, we performed colony-forming assays in STING-depleted human and murine tumor cell lines that were exposed to ionizing radiation. The shSTING cells displayed less growth suppression after a single 6 Gy radiation dose compared to shScrambled control (Supplementary Fig. S3B-F). Consistent with low endogenous STING expression, shSTING A549 cells displayed similar growth and radiation response to shScrambled control (Supplementary Fig. S3G). In turn, both primary and immortalized MEFs from STINGko mice exhibited higher viability compared to WT MEFs in response to IR (Supplementary Fig. S3H-I).

The striking number of STING-dependent genes involved in cell proliferation pointed to STING functions that have not been fully explored to date. Several STING-dependent genes were components of the CDKN1A/RB/MDM2 network (Fig. 3G), including the stoichiometric cyclin-dependent kinase inhibitor CDKN1A (p21, CIP1, WAF1), yielding a p-value of 2.2×10^{-35} and an activation z-score of −3.16, indicating strong repression in the absence of STING. Western blot analysis of wild type and STINGko primary and immortalized cell lines revealed that basal p21 expression was greater in WT than STINGko cells and p21 induction by IR was attenuated in the STINGko mutants (Fig. 3H–I and Supplementary Fig. S4A-B). Similarly, STING-depleted HCT116, and SCC61 tumor cells also expressed lower p21 compared to their shScrambled controls (Fig. 3J–K and Supplementary Fig. S4C-D). HEK293 cells overexpressing FLAG-tagged STING displayed modestly increased p21 expression and lower Rb phosphorylation compared to vector controls (Supplementary Fig. S4E). Confirming order of function between STING and p21, transient knockdown of p21 in HCT116 tumor cells using siRNA increased phosphorylated Rb but did not affect STING expression or phospho-TBK1 levels (Supplementary Fig. S4F), while transient siRNA-mediated knockdown of STING in wild-type MEFs attenuated p21 expression and worked as well as transient knockdown of p21 (Supplementary Fig. S4G), indicating that STING acts upstream of p21. Time-lapse imaging revealed enhanced proliferation in both untreated and irradiated p21 knockdown HCT116 cells (Fig. 3L), partly recapitulating the phenotype of shSTING cell lines. Live cell imaging of nuclei-stained tumor cells also revealed that transient knockdown of p21 in stable STING-depleted tumor

cell lines led to greater cell proliferation compared to their respective non-targeting controls (Supplementary Fig. S4H-J), suggesting that even though p21 acts as a downstream effector, STING only has partial control of p21.

STING-mediated regulation of CDKN1A requires both NF-κB and p53

Activated STING triggers the classical NF-κB (p50/p65 heterodimer) transcriptional response leading to induction of inflammatory mediators(1,29). NF-κB has also been implicated in transcriptional regulation of p21(30,31). We recently showed that, in response to DNA damage, NF-κB binds to a consensus element in the p21 promoter, and induces p21 expression in p53-deficient acute myeloid leukemia cells(27). In HEK293 cells transiently transfected with an NF-κB-dependent luciferase reporter along with a STING overexpression vector, treatment with cGAMP to induce STING led to a 6-fold increase in luciferase activity at 24 hours compared to vector control (Fig. 4A). Similarly, treating WT primary MEFs with 2'3'-cGAMP to induce STING led to upregulation of the NF-κB subunit p65 and phospho-p65 along with the expected increase in phospho-TBK1 and higher expression of STAT1 (Fig. 4B and Supplementary Fig. S5A). Expression of p21 displayed a similar pattern to p65. As expected, STINGko primary MEFs stimulated with cGAMP failed to induce up-regulation of phospho-TBK1, STAT1, phospho-p65, and p21 (Fig. 4C and Supplementary Fig. S5B). Likewise, STINGko MEFs displayed decreased phospho-p65 and lower p21 expression after IR (Fig. 4D and Supplementary Fig. S5C). Diminished p21 expression after IR was also observed in the NF-κB DNA binding domain-deficient $p50^{-/-}$ MEFs (Fig. 4E and Supplementary Fig. S5D). Taken together, our data demonstrate that STING-mediated regulation of p21 involves the canonical NF-kB pathway.

In response to IR-induced DNA damage, p21 is known to be predominantly regulated by p53(32). To test the relative involvement of both NF-κB and p53 in the transcriptional regulation of the p21 gene CDKN1A, we used luciferase reporter constructs driven by the CDKN1A promoter(27). When HCT116 cells were transfected with reporter constructs encoding a wild type (GGGactccCC) or mutated (AATactccCC) p65 RE and stimulated with cGAMP, the mutant p65 RE displayed decreased activation at 24 hours (Fig. 4F). When the p21 reporters were similarly transfected in $p53^{-/-}$ HCT116 cells, the wild-type p21 reporter was no longer induced by cGAMP and the mutant p65 RE reporter displayed reduced basal expression and no cGAMP induction. Taken together, our data indicate that STING regulates p21 activation through NF-κB and p53 to modulate cellular proliferation.

STING maintains chromosomal stability

Micronuclei accumulate in cells that enter mitosis with unrepaired chromosomal breaks following irradiation(33) and can be detected using the cytokinesis-block micronucleus (CBMN) assay(26). CBMN analysis detected micronuclei in both STINGko and WT MEFs after IR (Supplementary Fig. S6). Karyotyping metaphase cells from primary STINGko and WT MEFs at early passage detected greater aneuploidy in STINGko compared to WT MEFs, which was increased by IR (Fig. 5A). We have karyotyped a total of 40 metaphase cells each for unirradiated WT and STINGko primary MEFs, and 50 metaphase cells each for irradiated cells. Unirradiated primary WT MEFs displayed 19% aneuploidy which increased to 52% after 6 Gy while STINGko MEFS displayed 46% without IR and 64%

after 6 Gy. Both Fisher's exact test and Chi-squared test for a 2×2 contingency table were performed to determine statistical significance of data. For unirradiated WT and STINGko cells, the 2-tailed p-value were 0.0307 using Fisher's test and 0.017 using Chi-squared test, suggesting that the association between the groups and outcomes is statistically significant. After radiation treatment (6Gy), on the other hand, the outcomes were not statistically significant, as the calculated two-tailed p-value were 0.3111 and 0.2241 for Fisher's test and Chi-squared test, respectively. The response to IR was more drastic in WT compared to STINGko MEFs, and is consistent with our previous observation that STINGko MEFs exhibited higher viability compared to WT cells. Based on detecting cells that appeared to have failed to complete mitosis and increased ploidy, we used flow cytometry and dual BrdU/PI staining to monitor the degree of polyploidy in STINGko and WT MEFs and compared these cells to HCT116 depleted of either p53 or p21 (Fig. 5B–C and Supplementary Fig. S7A-C). Consistent with prior studies(34,35), p53-deficient HCT116 cells displayed increased polyploidy while p21 deficiency conferred a similar effect that was further enhanced after IR (Fig. 5C and Supplementary Fig. S7C). Western blot analysis revealed higher levels of BUB1 (Budding Uninhibited by Benzimidazoles 1) and MAD2L1 (Mitotic Arrest Deficient 2-like 1), key mitotic checkpoint proteins involved in controlling the alignment and segregation of sister chromatids during mitosis(36–38), in both STINGko and WT MEFs and HCT116 cells lacking either p21 or p53 (Supplementary Fig. S7D-F). Both BUB1 and MAD2L1 have been demonstrated to be negatively regulated by the p53-p21-DREAM (DP, Rb-like, E2F4m and MuvB) pathway, which function through the cell cycle-dependent element and promoter sites of several late cell cycle target genes(39). Chromatin immunoprecipitation (ChIP) data revealed that the E2F4 transcription factor failed to bind to the promoter region of BUB1 and MAD2L1 in either STING- or p21-depleted HCT116 cells, both at basal level and in response to IR (Supplementary Fig. S7G). This helps explain why BUB1 and MAD2L1 protein levels are up-regulated in the absence of STING and provides a key mechanism for p53-p21-mediated G2/M cell cycle arrest in response to genotoxic stress.

STING deficiency confers sensitivity to WEE1 inhibition

While p21 is effective at restraining progression at G1/S, it has limited impact at G2/M, where the STING-deficient cells displayed the most dramatic cell cycle defect. In the normal cell cycle, premature activation of the mitotic cyclin-dependent CDK1 (CDC2) is blocked during S phase and G2 by inhibitory Tyr15 phosphorylation by WEE1(40). DNA damage in S or G2 activates the checkpoint and inhibits Tyr15 dephosphorylation, delaying mitosis to allow time for repair. Western blot analysis showed that the Tyr15 phosphorylated CDK1 was lower in STINGko MEFs compared to WT both at the basal level and after IR (Fig. 5D and Supplementary Fig. S8A). Staining for mitochondria and DNA in STINGko MEFs suggested that both the cytoplasmic and nuclear volumes were markedly reduced compared to WT (Fig. 5E). Total nuclear area in both STINGko MEFs and shSTING D54 cells were significantly smaller, based on time-lapse imaging (Figs. 5F–G), suggesting that STINGko MEFs have a similar phenotype to *wee* mutants that are defective in protein regulators that normally prevent cells from dividing when they are too small(41). Although STINGko MEFs appeared to increase in size slightly after IR, the effect was markedly less than for WT cells (Fig. 5E–F).

Inhibition of the kinase WEE1 in combination with DNA-damaging agents is a promising strategy in cancer therapy(42). The resulting activation of CDK can induce replication stress(43) or premature mitotic entry(42) leading to mitotic catastrophe and cell death. We hypothesized that further impairing G2/M regulation in STING-deficient cells by blocking CDK1 Tyr15 phosphorylation by WEE1 might be differentially toxic and/or further sensitize the cells to IR. Time-lapse analysis of cell proliferation revealed that WEE1 inhibitor MK1775(42,44) conferred greater growth inhibition and enhanced the effects of IR on STINGko MEFs (Fig. 5H–I). A similar pattern was observed for shSTING D54, HCT116, and SCC61 (Fig. 5J–L). As expected, WEE1 inhibitor in combination with IR also inhibited cell proliferation in WT MEFs and shScrambled D54, HCT116, and SCC61 tumor cells (Supplementary Fig. S8B-E).

Discussion

We demonstrated that STING has cell-intrinsic functions in the regulation of the cell cycle and chromosomal stability. Depletion of STING conferred a shorter doubling time in all cell types compared to wild-type, implicating STING in cell-intrinsic control of proliferation and response to IR exposure. Our finding is consistent with recent data correlating STING suppression and poor prognosis in patients with hepatocellular carcinoma(45). RNA expressional profiling demonstrated that STING is involved in cell cycle control through CDKN1A. We further hypothesized a mechanistic link between STING and CDKN1A can be provided by NF-κB based on published observations that NF-κB transcriptionally activates CDKN1A(30,31). Here we provide the first evidence that both p65 and p53 are required for the STING-mediated activation of p21, implicating a previously unrecognized STING/NF-κB/p53/CDKN1A pathway in cell-intrinsic regulation of cell proliferation. This finding is consistent with a previous report demonstrating a high concentration of p65 transcription factor bound to the chromatin of senescent cells, and that senescence was bypassed using a combination of NF-κB inhibition and p53 inactivation(46). These results provide additional support to recent reports implicating the cGAS/STING pathway in regulation of senescence phenotype(14,17), as well as a previous study demonstrating that wild-type, but not STINGko mice, exhibited accelerated aging and massive hair greying three months after exposure to IR(18). However, our data indicate that STING regulates the G1/S transition independently from cGAS, because at least one of the cell lines tested (HCT116) does not express cGAS (see (22) and Fig. 3G).

Progression from G2 to M phase is driven by the activation of the CDK1/cyclin B1 complex(40). The phosphorylation of CDK1 on Thr14 and Tyr15 by Myt1 and Wee1 kinase, respectively, inhibits CDK1 activity during G2, while dephosphorylation by CDC25 phosphatase at these tyrosine sites enable progression through M phase(42). The CDK1/cyclin B1 heterodimer induces mitosis by activating enzymes involved in spindle assembly and mitosis-specific microtubule reorganization. Karyotypic analyses on primary MEFs revealed that the absence of STING led to a higher degree of chromosomal aberrations and polyploidy, and these aberrations are enhanced by IR. This result suggests that STING modulates entry to mitosis and consequently, the assembly of the mitotic spindle. We observed that STINGko MEFs exhibited lower levels of inactive CDK1 and higher levels of the mitotic checkpoint markers BUB1 and MAD2L1 compared to WT both at basal level

and in response to IR. Upregulation of BUB1 and MAD2L1 in tumor cells are associated with tumor cell proliferation(37,47,48). Analysis of normal and tumor samples from The Cancer Genome Atlas (TCGA) project demonstrated a positive correlation between high copy number variations and high expression of genes implicated in cell cycle regulation, G2/M checkpoints, mitosis, and chromosome maintenance, suggesting that there is increased proliferation in high aneuploid tumors(49). Taken together, our findings suggest a putative tumor-suppressive role for STING.

Micronuclei formation following genotoxic stress has been used as a marker for CIN(33). Double strand breaks in chromosomes give rise to chromatin fragments that do not segregate with the rest of the genome following mitosis, which eventually form into micronuclei(33). Micronuclei have been observed to spontaneously undergo nuclear envelope collapse in normal and tumor cells during interphase leading to the release of cytoplasmic DNA fragments that trigger cGAS/STING-mediated innate immune activation of cytokines and chemokines(15,16). Both WT and STINGko MEFs exposed to IR were observed to form micronuclei (Supplementary Fig. S6), but STINGko cells exhibited higher degree of CIN than WT (Fig. 5A), presumably as a result of its inability to sense local danger signals. Consequently, STING-depleted cells will continue to exhibit a deregulated cell cycle, accumulate errors in their genome, and fail to activate host immune proinflammatory responses. This is consistent with previous reports demonstrating that the cGAS-STING pathway is critical for the induction of inflammatory cytokines and chemokines that modulate the host immune responses(14,17,18). Our findings help shed light on the connection between accumulation of nuclear structure abnormalities in tumor cells and the mechanisms that they employ to evade host-mediated immune responses. However, in contrast to our results, Bakhoum *et al.*(50) reported that continuous chromosome segregation errors promoted tumor metastasis through cGAS-STING – mediated activation of non-canonical NF-kB following recognition of accumulated cytosolic DNA. This correlated with a shorter disease-free survival in breast and lung cancer patients(50). The discrepancy between our findings and their study suggest that STING may be a tumor suppressor in certain tumor types but could have tumor-promoting effects in others. These paradoxical roles of STING warrant further investigation.

Quantifying STING expression in tumor samples might be useful in precision oncology in that alternative modes of killing or greater radiation doses might be required in STINGko tumors due to increased perturbations in cell cycle regulation that favors tumor survival. Additionally, since most normal cells express STING and many tumor cells do not, this difference might be exploited in cancer therapy. It is postulated that induction of mitotic catastrophe through WEE1 inhibition may be used as radiosensitizers in the clinical setting(42). We demonstrated that STING-depleted cells treated with the WEE1 inhibitor MK1775 in combination with IR exhibited cell growth delay compared to WT control. WEE1 inhibitors have been shown to trigger mitotic entry prior to completion of DNA synthesis and DNA damage repair, which can lead to mitotic catastrophe and cell death(42). Downregulation of WEE1 also leads to elevated CDK activity during S Phase, resulting to replication stress(43). Considering current findings regarding frequent deletion/suppression of cGAS/STING pathway in tumor cells, our data pose important questions about tumor suppressive functions of STING as a potential “gatekeeper” or homeostatic regulator, the

absence of which may be associated with early stages of oncogenesis(12). Further investigations on the regulation and function of STING in normal and cancer cells are warranted by these insights and may provide additional therapeutic targets to help improve cancer therapy.

Supplementary Material

Refer to Web version on PubMed Central for supplementary material.

Acknowledgements

The authors would like to thank Rolando Torres, Michael Beckett, Dr. Giovanna Bernal, Dr. Longtao Wu, and Dr. David Hosfield for technical assistance; Amy K. Huser for assistance in manuscript preparation; Dr. David J. Grdina for intellectual discussions; Dr. Michael Spiotto and Dr. Geoffrey Greene for sharing reagents and equipment; Yue Liu for critical reading of the manuscript; Dr. Pieter Farber and the Functional Genomics Facility staff; Dr. Vytas Bindokas, Shirley Bond, and Dr. Christine Labno of the Integrated Microscopy Core Facility; and Dr. Siquan Chen of the Cellular Screening Center.

Financial Support: This work was supported by the Virginia and D.K. Ludwig Fund for Cancer Research (D.K. Ludwig Fund) to R.R. Weichselbaum, Varian Medical Systems grant to R.R. Weichselbaum, the Lung Cancer Research Foundation grant to R.R. Weichselbaum, and the NIH NCI RO1 grant (CA199663) to S.J. Kron.

References

1. Ishikawa H, Barber GN. STING is an endoplasmic reticulum adaptor that facilitates innate immune signalling. Nature 2008;455(7213):674–8. [PubMed: 18724357]
2. Ishikawa H, Ma Z, Barber GN. STING regulates intracellular DNA-mediated, type I interferon-dependent innate immunity. Nature 2009;461(7265):788–92 10.1038/nature08476. [PubMed: 19776740]
3. Saitoh T, Fujita N, Hayashi T, Takahara K, Satoh T, Lee H, et al. Atg9a controls dsDNA-driven dynamic translocation of STING and the innate immune response. Proceedings of the National Academy of Sciences of the United States of America 2009;106(49):20842–6 10.1073/pnas.0911267106. [PubMed: 19926846]
4. Zhong B, Yang Y, Li S, Wang Y-Y, Li Y, Diao F, et al. The adaptor protein MITA links virus-sensing receptors to IRF3 transcription factor activation. Immunity 2008;29(4):538–50. [PubMed: 18818105]
5. Liu S, Cai X, Wu J, Cong Q, Chen X, Li T, et al. Phosphorylation of innate immune adaptor proteins MAVS, STING, and TRIF induces IRF3 activation. Science (New York, NY) 2015;347(6227):aaa2630.
6. Burdette DL, Monroe KM, Sotelo-Troha K, Iwig JS, Eckert B, Hyodo M, et al. STING is a direct innate immune sensor of cyclic di-GMP. Nature 2011;478(7370):515–8 10.1038/nature10429. [PubMed: 21947006]
7. Wu J, Sun L, Chen X, Du F, Shi H, Chen C, et al. Cyclic GMP-AMP is an endogenous second messenger in innate immune signaling by cytosolic DNA. Science (New York, NY) 2013;339(6121):826–30 10.1126/science.1229963.
8. Gao P, Ascano M, Wu Y, Barchet W, Gaffney BL, Zillinger T, et al. Cyclic [G(2',5')pA(3',5')p] is the metazoan second messenger produced by DNA-activated cyclic GMP-AMP synthase. Cell 2013;153(5):1094–107 10.1016/j.cell.2013.04.046. [PubMed: 23647843]
9. Sun L, Wu J, Du F, Chen X, Chen ZJ. Cyclic GMP-AMP synthase is a cytosolic DNA sensor that activates the type I interferon pathway. Science (New York, NY) 2013;339(6121):786–91 10.1126/science.1232458.
10. Ablasser A, Goldeck M, Cavlar T, Deimling T, Witte G, Rohl I, et al. cGAS produces a 2'–5'-linked cyclic dinucleotide second messenger that activates STING. Nature 2013;498(7454):380–4 10.1038/nature12306. [PubMed: 23722158]

11. Bernier J, Hall EJ, Giaccia A. Radiation oncology: a century of achievements. Nature reviews Cancer 2004;4(9):737–47 10.1038/nrc1451. [PubMed: 15343280]
12. Hanahan D, Weinberg RA. The hallmarks of cancer. Cell 2000;100(1):57–70. [PubMed: 10647931]
13. Bakhoum SF, Compton DA. Chromosomal instability and cancer: a complex relationship with therapeutic potential. The Journal of clinical investigation 2012;122(4):1138–43 10.1172/JCI59954. [PubMed: 22466654]
14. Yang H, Wang H, Ren J, Chen Q, Chen ZJ. cGAS is essential for cellular senescence. Proceedings of the National Academy of Sciences 2017;114(23):E4612–E20 10.1073/pnas.1705499114.
15. Harding SM, Benci JL, Irianto J, Discher DE, Minn AJ, Greenberg RA. Mitotic progression following DNA damage enables pattern recognition within micronuclei. Nature 2017;548(7668):466–70 10.1038/nature23470 [PubMed: 28759889]
16. Mackenzie KJ, Carroll P, Martin C-A, Murina O, Fluteau A, Simpson DJ, et al. cGAS surveillance of micronuclei links genome instability to innate immunity. Nature 2017;548:461 10.1038/nature23449 [PubMed: 28738408]
17. Gluck S, Guey B, Gulen MF, Wolter K, Kang T-W, Schmacke NA, et al. Innate immune sensing of cytosolic chromatin fragments through cGAS promotes senescence. Nat Cell Biol 2017;19(9):1061–70 10.1038/ncb3586 [PubMed: 28759028]
18. Dou Z, Ghosh K, Vizioli MG, Zhu J, Sen P, Wangensteen KJ, et al. Cytoplasmic chromatin triggers inflammation in senescence and cancer. Nature 2017;550:402 10.1038/nature24050 [PubMed: 28976970]
19. Corrales L, Glickman LH, McWhirter SM, Kanne DB, Sivick KE, Katibah GE, et al. Direct Activation of STING in the Tumor Microenvironment Leads to Potent and Systemic Tumor Regression and Immunity. Cell reports 2015;11(7):1018–30 10.1016/j.celrep.2015.04.031. [PubMed: 25959818]
20. Woo SR, Fuertes MB, Corrales L, Spranger S, Furdyna MJ, Leung MY, et al. STING-dependent cytosolic DNA sensing mediates innate immune recognition of immunogenic tumors. Immunity 2014;41(5):830–42 10.1016/j.immuni.2014.10.017. [PubMed: 25517615]
21. Deng L, Liang H, Xu M, Yang X, Burnette B, Arina A, et al. STING-Dependent Cytosolic DNA Sensing Promotes Radiation-Induced Type I Interferon-Dependent Antitumor Immunity in Immunogenic Tumors. Immunity 2014;41(5):843–52 10.1016/j.immuni.2014.10.019. [PubMed: 25517616]
22. Xia T, Konno H, Ahn J, Barber GN. Deregulation of STING Signaling in Colorectal Carcinoma Constrains DNA Damage Responses and Correlates With Tumorigenesis. Cell reports 2016;14(2):282–97 10.1016/j.celrep.2015.12.029. [PubMed: 26748708]
23. Xia T, Konno H, Barber GN. Recurrent Loss of STING Signaling in Melanoma Correlates with Susceptibility to Viral Oncolysis. Cancer research 2016;76(22):6747–59 10.1158/0008-5472.can-16-1404. [PubMed: 27680683]
24. Uhlen M, Zhang C, Lee S, Sjöstedt E, Fagerberg L, Bidkhori G, et al. A pathology atlas of the human cancer transcriptome. Science (New York, NY) 2017;357(6352) 10.1126/science.aan2507.
25. Ranoa DR, Parekh AD, Pitroda SP, Huang X, Darga T, Wong AC, et al. Cancer therapies activate RIG-I-like receptor pathway through endogenous non-coding RNAs. Oncotarget 2016;7(18):26496–515 10.18632/oncotarget.8420. [PubMed: 27034163]
26. Fenech M Cytokinesis-block micronucleus cytome assay. Nature Protocols 2007;2:1084 10.1038/nprot.2007.77. [PubMed: 17546000]
27. Nicolae CM, O'Connor MJ, Constantin D, Moldovan G-L. NFκB regulates p21 expression and controls DNA damage-induced leukemic differentiation. Oncogene 2018 10.1038/s41388-018-0219-y.
28. Begg AC, McNally NJ, Shrieve DC, Kärche H. A method to measure the duration of DNA syntheses and the potential doubling time from a single sample. Cytometry 1985;6(6):620–6 10.1002/cyto.990060618. [PubMed: 4064842]
29. Hayden MS, Ghosh S. Signaling to NF-κB. Genes & development 2004;18(18):2195–224 10.1101/gad.1228704. [PubMed: 15371334]

30. Basile JR, Eichten A, Zacny V, Münger K. NF-κB-mediated induction of p21 Cip1/waf1 by tumor necrosis factor α induces growth arrest and cytoprotection in normal human keratinocytes. Molecular Cancer Research 2003;1(4):262–70. [PubMed: 12612054]

31. Hinata K, Gervin AM, Zhang YJ, Khavari PA. Divergent gene regulation and growth effects by NF-κB in epithelial and mesenchymal cells of human skin. Oncogene 2003;22(13):1955–64. [PubMed: 12673201]

32. El-Deiry WS, Tokino T, Velculescu VE, Levy DB, Parsons R, Trent JM, et al. WAF1, a potential mediator of p53 tumor suppression. Cell 1993;75(4):817–25 10.1016/0092-8674(93)90500-P. [PubMed: 8242752]

33. Heddle JA, Carrano AV. The DNA content of micronuclei induced in mouse bone marrow by γ-irradiation: evidence that micronuclei arise from acentric chromosomal fragments. Mutation Research/Fundamental and Molecular Mechanisms of Mutagenesis 1977;44(1):63–9 10.1016/0027-5107(77)90115-4. [PubMed: 331097]

34. Fujiwara T, Bandi M, Nitta M, Ivanova EV, Bronson RT, Pellman D. Cytokinesis failure generating tetraploids promotes tumorigenesis in p53-null cells. Nature 2005;437:1043 10.1038/nature04217 [PubMed: 16222300]

35. Bunz F, Dutriaux A, Lengauer C, Waldman T, Zhou S, Brown JP, et al. Requirement for p53 and p21 to Sustain G2 Arrest After DNA Damage. Science (New York, NY) 1998;282(5393):1497–501 10.1126/science.282.5393.1497.

36. Hanks S, Coleman K, Reid S, Plaja A, Firth H, FitzPatrick D, et al. Constitutional aneuploidy and cancer predisposition caused by biallelic mutations in BUB1B. Nature genetics 2004;36:1159 10.1038/ng1449. [PubMed: 15475955]

37. Sotillo R, Schvartzman J-M, Socci ND, Benezra R. Mad2-induced chromosome instability leads to lung tumour relapse after oncogene withdrawal. Nature 2010;464:436 10.1038/nature08803 [PubMed: 20173739]

38. Cahill DP, Lengauer C, Yu J, Riggins GJ, Willson JKV, Markowitz SD, et al. Mutations of mitotic checkpoint genes in human cancers. Nature 1998;392:300 10.1038/32688. [PubMed: 9521327]

39. Fischer M, Quaas M, Steiner L, Engeland K. The p53-p21-DREAM-CDE/CHR pathway regulates G2/M cell cycle genes. Nucleic Acids Research 2016;44(1):164–74 10.1093/nar/gkv927. [PubMed: 26384566]

40. Parker L, Piwnica-Worms H. Inactivation of the p34cdc2-cyclin B complex by the human WEE1 tyrosine kinase. Science (New York, NY) 1992;257(5078):1955–7 10.1126/science.1384126.

41. Nurse P, Thuriaux P. REGULATORY GENES CONTROLLING MITOSIS IN THE FISSION YEAST SCHIZOSACCHAROMYCES POMBE. Genetics 1980;96(3):627–37. [PubMed: 7262540]

42. De Witt Hamer PC, Mir SE, Noske D, Van Noorden CJF, Würdinger T. WEE1 Kinase Targeting Combined with DNA-Damaging Cancer Therapy Catalyzes Mitotic Catastrophe. Clinical Cancer Research 2011;17(13):4200–7 10.1158/1078-0432.Ccr-10-2537. [PubMed: 21562035]

43. Beck H, Nähse-Kumpf V, Larsen MSY, O'Hanlon KA, Patzke S, Holmberg C, et al. Cyclin-Dependent Kinase Suppression by WEE1 Kinase Protects the Genome through Control of Replication Initiation and Nucleotide Consumption. Molecular and cellular biology 2012;32(20): 4226–36 10.1128/MCB.00412-12. [PubMed: 22907750]

44. Kreahling JM, Foroutan P, Reed D, Martinez G, Razabdouski T, Bui MM, et al. Wee1 Inhibition by MK-1775 Leads to Tumor Inhibition and Enhances Efficacy of Gemcitabine in Human Sarcomas. PloS one 2013;8(3):e57523 10.1371/journal.pone.0057523. [PubMed: 23520471]

45. Bu Y, Liu F, Jia QA, Yu SN. Decreased Expression of TMEM173 Predicts Poor Prognosis in Patients with Hepatocellular Carcinoma. PloS one 2016;11(11):e0165681 10.1371/journal.pone. 0165681. [PubMed: 27814372]

46. Chien Y, Scuoppo C, Wang X, Fang X, Balgley B, Bolden JE, et al. Control of the senescence-associated secretory phenotype by NF-kappaB promotes senescence and enhances chemosensitivity. Genes & development 2011;25(20):2125–36 10.1101/gad.17276711. [PubMed: 21979375]

47. Grabsch H, Takeno S, Parsons WJ, Pomjanski N, Boecking A, Gabbert HE, et al. Overexpression of the mitotic checkpoint genes BUB1, BUBR1, and BUB3 in gastric cancer--association with

tumour cell proliferation. The Journal of pathology 2003;200(1):16–22 10.1002/path.1324. [PubMed: 12692836]

48. Wang Z, Katsaros D, Shen Y, Fu Y, Canuto EM, Benedetto C, et al. Biological and Clinical Significance of MAD2L1 and BUB1, Genes Frequently Appearing in Expression Signatures for Breast Cancer Prognosis. PloS one 2015;10(8):e0136246 10.1371/journal.pone.0136246. [PubMed: 26287798]
49. Davoli T, Uno H, Wooten EC, Elledge SJ. Tumor aneuploidy correlates with markers of immune evasion and with reduced response to immunotherapy. Science (New York, NY) 2017;355(6322) 10.1126/science.aaf8399.
50. Bakhoum SF, Ngo B, Laughney AM, Cavallo J-A, Murphy CJ, Ly P, et al. Chromosomal instability drives metastasis through a cytosolic DNA response. Nature 2018 10.1038/nature25432

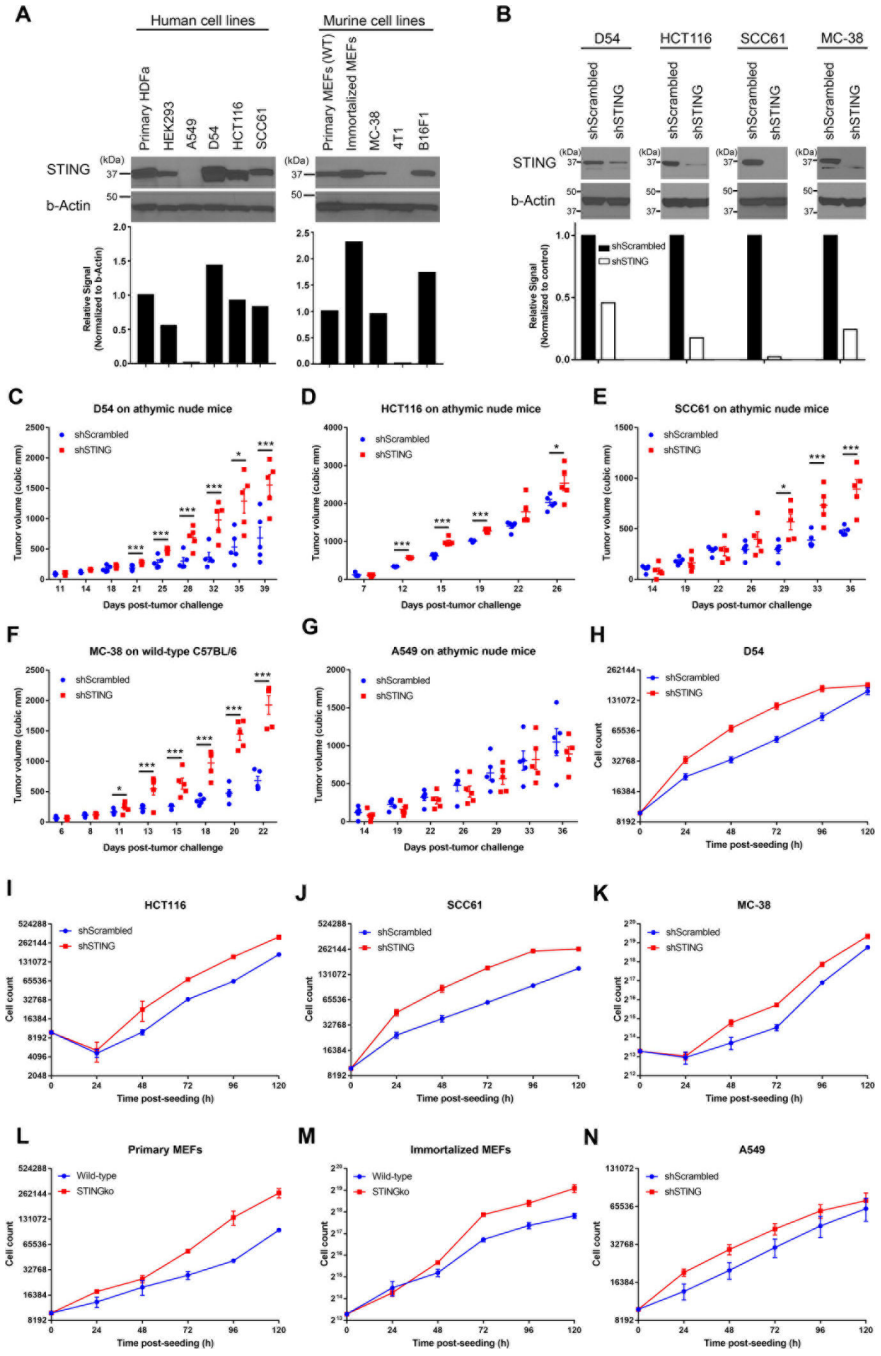

Figure 1. STING controls tumor growth in a cell-intrinsic mode.

(A) Western blot analysis of STING expression in various human and mice cell lines. Bottom panel are quantified bands normalized to b-Actin control. **(B)** Western blot analyses of lysates from stable D54, HCT116, SCC61, and MC-38 tumor cell lines expressing short hairpin RNAs targeting STING (shSTING) or scrambled control (shScrambled). Bottom panel are quantified bands normalized to b-Actin and their respective non-targeting controls. (**C-E**) Tumor growth of shSTING knockdown and shScrambled control D54 **(C)**; HCT116 **(D)**; and SCC61 **(E)** cell lines in athymic nude mice. **(F)** Tumor growth of MC-38 shSTING

knockdown in WT C57BL/6 mice. **(G)** Tumor growth of A549 with shSTING knockdown in athymic nude mice. Tumor model data are representative of three experiments, each with n = 5 mice per group. **(H-N)** Kinetic analysis of STING-depleted human tumor cell lines D54 **(H)**, HCT116 **(I)**, and SCC61 **(J)** as well as murine cell lines MC-38 **(K)**, primary WT and STINGko MEFs **(L)**, and SV40-immortalized WT and STINGko MEFs **(M)** proliferation in vitro were measured over time by manual cell counting. STING-depleted A549 cells were also tested as negative control **(N)**. In vitro growth curve data are representative of at least three experiments, each with n = 3 per group. P-values were determined using unpaired Student's t-test. Error bars are SEM. *P < 0.05, **P < 0.01, ***P < 0.005.

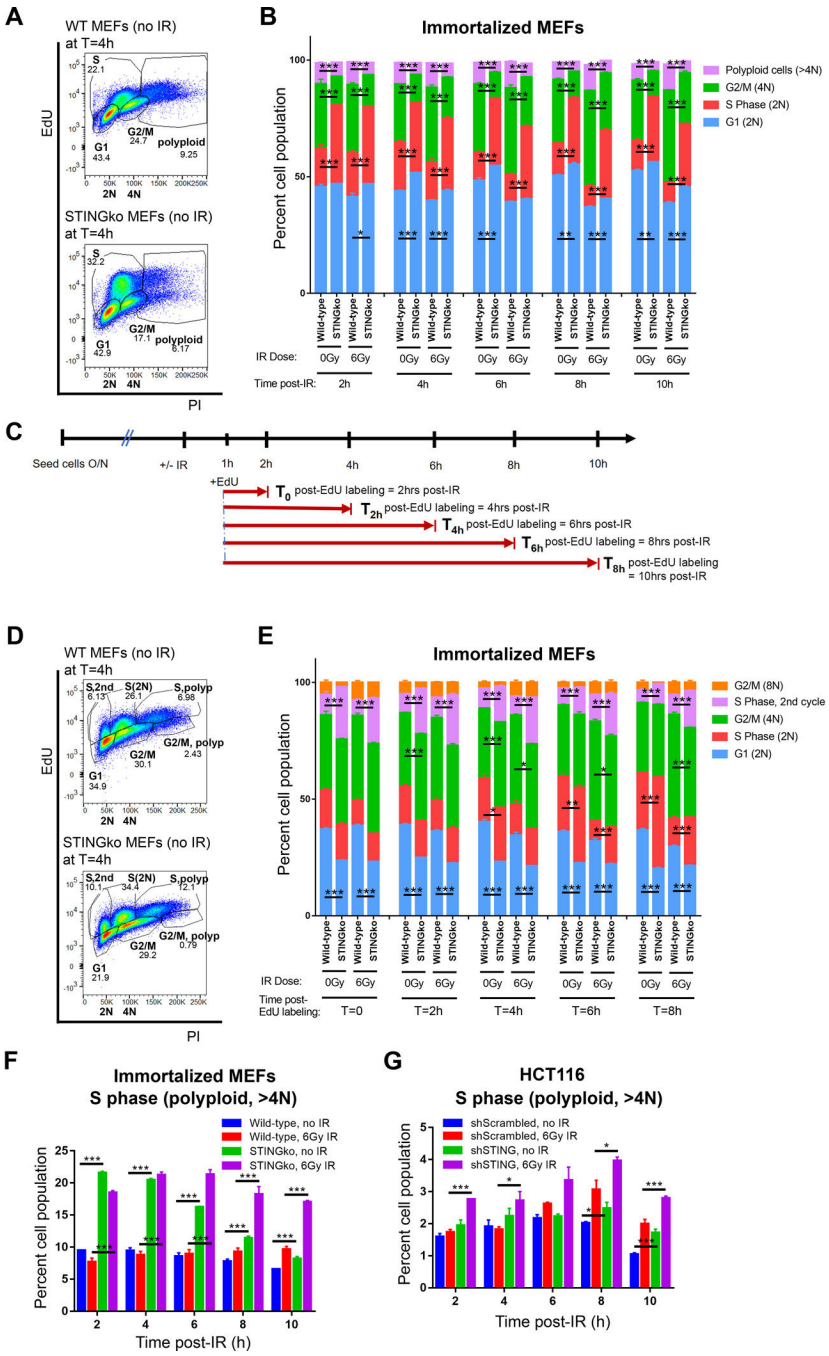

Figure 2. STING-dependent regulation of proliferation is associated with perturbations of cell cycle.

(A) Gating strategy performed on EdU^+ and PI^+ double-labeled WT (top panel) and STINGko (bottom panel) single cells to identify cell population in G1 (2N), G2/M (4N), S (≥2N, ≤4N), and polyploid cells (>4N). **(B)** Bar graph representing the percentage of cells in G1 phase, S phase, G2/M phase over time at baseline and in response to IR. **(C)** Schematic diagram of chase-EdU labeling experiment performed on WT and STINGko MEFs. EdU was added to cells one hour post-IR. Cell were harvested at indicated time points for

processing. **(D)** Gating strategy performed on EdU^+ and PI^+ double-labeled WT (top panel) and STINGko (bottom panel) single cells to identify cell population in G1 (2N), G2/M (4N), S (≥2N, ≤4N), S phase in second cycle (EdU+ cells at the 2N peak), and polyploid cells (>4N). **(E)** Bar graph representing the percentage of WT and STINGko cells in G1, G2/M, S phase, and cells in S phase of the second cycle at baseline and in response to IR. **(F-G)** Bar graph representing the percentage of polyploid cells in WT and STINGko MEFs **(F)** and shSTING HCT116 **(G)** over time at baseline and in response to IR. Data are representative of at least two experiments, with each condition done in triplicates. P-values were determined using unpaired Student's t-test. Error bars are SEM. *P < 0.05, **P < 0.01, ***P < 0.005.

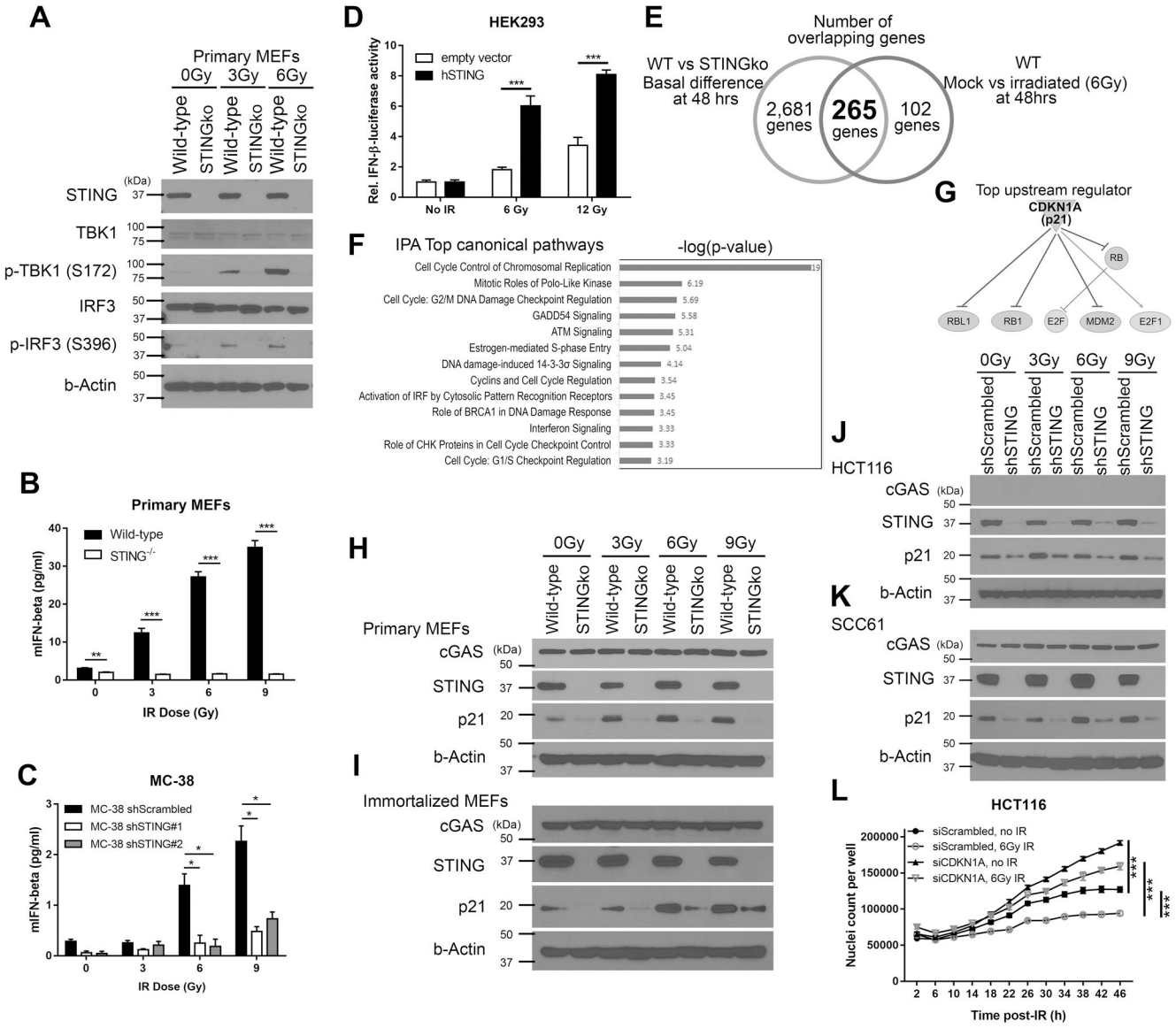

Figure 3. STING controls CDKN1A-dependent pathways of cell cycle regulation.

(A) Western analyses of lysates from WT and STING$^{-/-}$ primary MEFs 48 hours post-exposure to increasing doses of IR. The membranes were probed for STING, TBK1, phospho-TBK1 Ser172, IRF3, and phosphor-IRF3 Ser396. B-actin antibody was used for loading control. **(B)** IFN-β protein level in WT and STING$^{-/-}$ MEFs supernatant 48 hours following exposure to increasing doses of IR. **(C)** IFN- β protein secretion in MC-38 with stable shSTING knockdown 48 hours following exposure to increasing doses of IR. **(D)** Overexpression of STING in HEK293 cells led to a higher IFN-β promoter-driven induction of luciferase activity following exposure to increasing IR dose. **(E)** Transcriptional profiling of C57BL/6 wild-type (WT) and STINGko primary MEFs 48 hours following 0 or 6 Gy. Venn diagram displays the number of overlapping differentially expressed genes (DEGs) between the basal differences in WT vs. STINGko MEFs and the effects of irradiation in WT MEFs. **(F)** Top-ranked cellular pathway classification of the 265 DEGs that are

activated by IR in WT and STINGko MEFs analyzed using Ingenuity Pathway Analysis (IPA). **(G)** CDKN1A was predicted as a top upstream regulator that potentially affects most of the 265 DEGs analyzed using IPA Upstream Analysis. **(H-K)** Western analyses of STING and p21 expression in lysates from primary WT and STINGko MEFs **(H)**, SV40-immortalized WT and STINGko MEFs **(I)**, shSTING HCT116 **(J)**, and shSTING SCC61 **(K)** harvested 48 hours post-exposure to increasing doses of IR. **(L)** Kinetic analysis of siCDKN1A HCT116 proliferation *in vitro* were measured over time in response to 6 Gy IR using the IncuCyte live cell imaging system. *In vitro* growth curve data are representative of at least two experiments, each with n = 3 per group. P-values were determined using unpaired Student's t-test. Error bars are SEM. *P < 0.05, **P < 0.01, ***P < 0.005.

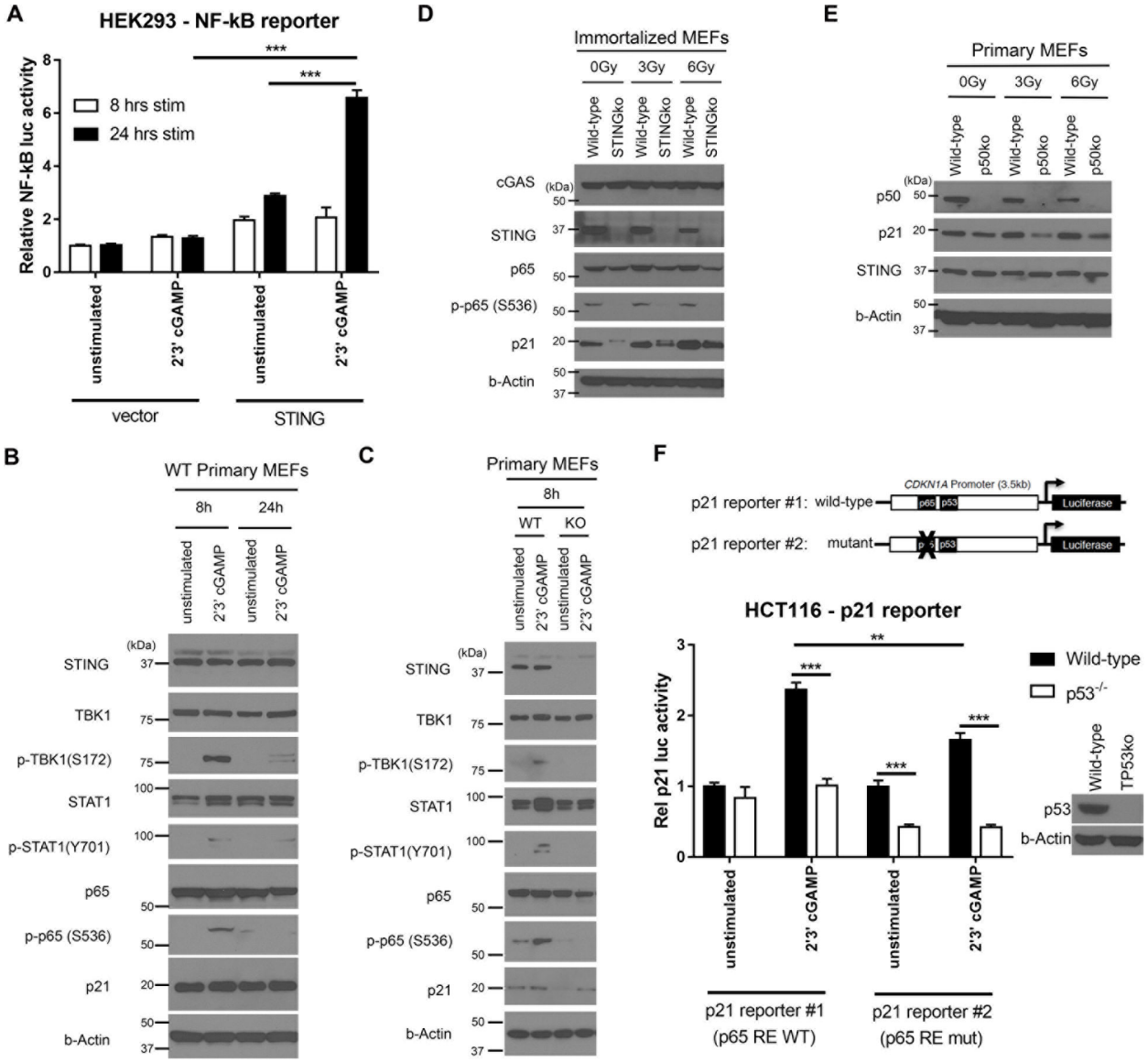

Figure 4. STING activates CDKN1A in an NF-κB/p53-dependent manner.

(A) Overexpression of STING in HEK293 cells led to a higher NF-κB promoter-driven induction of luciferase activity at 8- and 24-hours following stimulation with 2'3'-cGAMP. **(B-C)** Western analysis of lysates isolated from WT primary MEFs **(B)** and STINGko primary MEFs **(C)** that were stimulated with 2'3'-cGAMP STING-specific agonist at different time points to demonstrate STAT1, NF-κB p65 subunit, and p21 activation. **(D)** Western analyses of lysates from immortalized WT and STINGko MEFs 48 hours post-exposure to increasing IR dose. **(E)** Western analyses of lysates from WT and $p50^{-/-}$ primary MEFs 48 hours post-exposure to increasing IR dose. **(F)** WT and $p53^{-/-}$ HCT116 cells were transiently transfected with either a wild-type (reporter #1) or p65 binding-deficient (reporter #2) CDKN1A promoter-driven luciferase construct. Induction of luciferase activity was measured 24 hours post-stimulation with 2'3'-cGAMP. Data are

representative of at least three experiments. P-values were determined using unpaired Student's t-test. Error bars are SEM. *P < 0.05, **P < 0.01, ***P < 0.005.

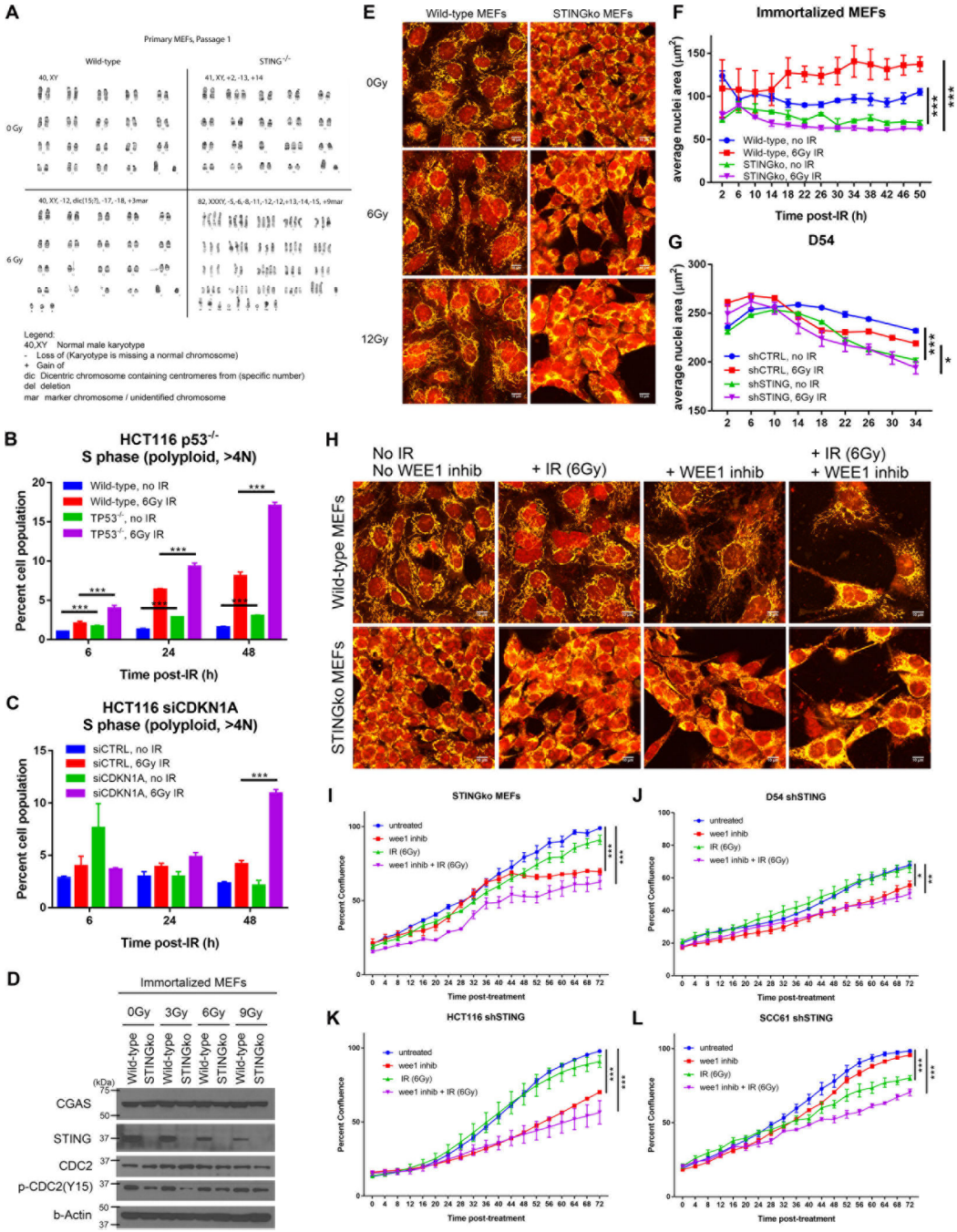

Figure 5. STING regulates mitotic checkpoint and chromosomal stability.

(A) Representative images of chromosome analysis performed on G-banded metaphase cells from primary WT and STINGko MEFs in passage 1 that were either mock-irradiated or treated with 6 Gy IR. **(B-C)** Bar graph representing the percentage of polyploid cells in BrdU/PI double-labeled $p53^{-/-}$ **(B)** and p21-depleted **(C)** HCT116 cell lines. **(D)** Western analyses of cGAS, STING, and phospho CDC2 Tyr15 expression in lysates from WT and STINGko MEFs harvested 48 hours post-exposure to increasing IR doses. **(E)** WT and STINGko MEFs at 48 hours post-treatment with increasing IR dose, stained for DNA and

mitochondrial/cytoplasmic compartments using Draq5 and MitoTracker Red, respectively; scale bar, 10 μm. **(F-G)** Kinetic analysis of average nuclear area of MEFs **(F)** and D54 tumor cells **(G)** stained with Nuclight Red dye measured over time at baseline and in response to IR. **(H)** WT and STINGko MEFs treated with WEE1 inhibitor MK1775 in combination with IR (6 Gy) were stained for DNA and mitochondrial/cytoplasmic compartments using Draq5 and MitoTracker Red, respectively at 48 hours post-treatment; scale bar, 10 μm. **(I-L)** Kinetic analysis of STINGko MEFs **(I)** as well as shSTING D54 **(J)**, HCT116 **(K)**, and SCC61 **(L)** proliferation *in vitro* were measured over time in response to WEE1 inhibitor MK1775 ± IR (6 Gy) using the IncuCyte live cell imaging system. *In vitro* growth curve data are representative of at least three experiments, each with n = 3 per group. P-values were determined using unpaired Student's t-test. Error bars are SEM. *P < 0.05, **P < 0.01, ***P < 0.005.

Table I.

Quantification of tumor proliferation in 3D murine models.

Cell Line	Cell type and origin	Genetic Modification	Linear equation of growth curve	Time (X) required to reach a tumor volume (Y) of 300 cubic mm	Average	Std Dev	Student's t-test
D54	Glioblastoma multiforme, human	shScrambled	Y = 39.32*X - 486.2	19.995	28.272	8.348	0.034
			Y = 11.14*X + 5.631	26.425			
			Y = 27.08*X - 353.6	24.136			
			Y = 6.53*X + 25.5	42.037			
			Y = 14.7*X - 122.9	28.769			
		shSTING	Y = 63.35*X - 839.6	17.989	18.673	0.973	
			Y = 42.27*X - 473	18.287			
			Y = 29.24*X - 296.3	20.393			
			Y = 59.49*X - 790	18.322			
			Y = 72.27*X - 1028	18.376			
HCT116	Colon adenocarcinoma, human	shScrambled	Y = 101.1*X - 801.1	10.891	10.695	0.244	0.000
			Y = 111.4*X - 926.1	11.006			
			Y = 93.52*X - 676.3	10.439			
			Y = 102.4*X - 788.1	10.626			
			Y = 97.06*X - 720.5	10.514			

Cell Line	Cell type and origin	Genetic Modification	Linear equation of growth curve	Time (X) required to reach a tumor volume (Y) of 300 cubic mm	Average	Std Dev	Student's t-test
		shSTING	Y = 98.96*X - 598.3	9.077	9.468	0.301	
			Y = 118.8*X - 804.6	9.298			
			Y = 115.2*X - 797.2	9.524			
			Y = 157.5*X - 1206	9.562			
			Y = 129.8*X - 982.2	9.878			
SCC61	Head and neck squamous carcnimoa, human	shScrambled	Y = 13.02*X - 54.28	27.210	26.392	2.737	0.042
			Y = 19.79*X - 178.8	24.194			
			Y = 13.68*X - 116.6	30.453			
			Y = 14.32*X - 37.58	23.574			
			Y = 15.61*X - 114.1	26.528			
		shSTING	Y = 40.08*X - 556.6	21.372	22.196	2.765	
			Y = 24.08*X - 301.6	24.983			
			Y = 42.24*X - 608.3	21.776			
			Y = 37.32*X - 619.8	24.646			
			Y = 45.73*X - 532.4	18.202			
MC-38	Colon adenocarcinoma, murine	shScrambled	Y = 30.65*X - 148.2	14.623	14.686	1.829	0.001

Cell Line	Cell type and origin	Genetic Modification	Linear equation of growth curve	Time (X) required to reach a tumor volume (Y) of 300 cubic mm	Average	Std Dev	Student's t-test
			Y = 41.99*X - 267.5	13.515			
			Y = 24.87*X - 125.3	17.101			
			Y = 43.22*X - 237.7	12.441			
			Y = 30.74*X - 184.1	15.748			
		shSTING	Y = 86.45*X - 570	10.064	10.167	0.563	
			Y = 128.6*X - 963.3	9.823			
			Y = 122.6*X - 1068	11.158			
			Y = 103.3*X - 728.8	9.959			
			Y = 120*X - 879.9	9.833			
A549	Alveolar basal epithelial cells, human	shScrambled	Y = 23.06*X - 327.4	27.207	21.126	3.470	0.659
			Y = 64.7*X - 892.3	18.428			
			Y = 33.01*X - 352.8	19.776			
			Y = 43.69*X - 582.2	20.192			
			Y = 44.87*X - 598.5	20.025			
		shSTING	Y = 40.08*X - 556.6	21.372	22.042	2.815	
			Y = 24.08*X - 301.6	24.983			

Cell Line	Cell type and origin	Genetic Modification	Linear equation of growth curve	Time (X) required to reach a tumor volume (Y) of 300 cubic mm	Average	Std Dev	Student's t-test
			Y = 50.75*X - 766.1	21.007			
			Y = 37.32*X - 619.8	24.646			
			Y = 45.73*X - 532.4	18.202			

Table II.

Depletion of STING in fibroblast and tumor cells altered the growth rate and the cell doubling time.

Cell Line	Cell type and origin	Model: Linear equation from a semi-log plot				Model: Non-linear calculation from a linear plot			
		Genetic Modification	Linear fit for the exponential part of the curve	growth rate, μ	R square	rate constant, k	k Standard error	Doubling time, ln(2)/K, hr	p-value
Primary MEFs	Fibroblast, murine	WT	Y = 0.01591*X + 9.105	0.016	1.000	0.018	0.00043	38.43	<0.0001
		STINGko	Y = 0.02809*X + 8.971	0.028	0.966	0.023	0.00029	30.01	
Immortalized MEFs	Fibroblast, murine	WT	Y = 0.03314*X + 9.113	0.033	0.961	0.027	0.00050	25.72	<0.0001
		STINGko	Y = 0.05233*X + 8.53	0.052	0.984	0.034	0.00059	20.31	
MC38	Colon adenocarcinoma, murine	shScrambled	Y = 0.03712*X + 7.819	0.037	0.917	0.031	0.00055	23.40	0.0030
		shSTING	Y = 0.04493*X + 7.938	0.045	0.981	0.033	0.00040	20.84	
D54	Glioblastoma multiforme, human	shScrambled	Y = 0.01908*X + 9.545	0.019	0.996	0.023	0.00025	30.62	0.0305
		shSTING	Y = 0.0225*X + 9.965	0.023	0.983	0.025	0.00077	27.65	
HCT116	Colon adenocarcinoma, human	shScrambled	Y = 0.9974*X + 0.2286	0.997	0.974	0.023	0.00050	30.31	<0.0001
		shSTING	Y = 1.309*X - 2.33	1.309	0.927	0.028	0.00052	24.40	
SCC61	Head and neck squamous carcnimoa, human	shScrambled	Y = 0.01891*X + 9.658	0.019	0.999	0.023	0.00025	30.04	<0.0001

Cell Line	Cell type and origin	Model: Linear equation from a semi-log plot				Model: Non-linear calculation from a linear plot			
		Genetic Modification	Linear fit for the exponential part of the curve	growth rate, μ	R square	rate constant, k	k Standard error	Doubling time, ln(2)/K, hr	p-value
		shSTING	Y = 0.02352*X + 10.22	0.024	0.994	0.029	0.00085	24.11	
A549	Alveolar basal epithelial cells, human	shScrambled	Y = 0.01639*X + 9.121	0.016	1.000	0.017	0.00030	40.88	0.5770
		shSTING	Y = 0.01548*X + 9.53	0.015	0.997	0.017	0.00055	39.96	